Serrano, J.; Arnau Martínez, FJ.; Bares-Moreno, P.; Gómez-Vilanova, A.; Garrido-Requena, J.; Luna-Blanca, MJ.; Contreras-Anguita, FJ. (2021). Analysis of a novel concept of 2-stroke rod-less opposed pistons engine (2S-ROPE): Testing, modelling, and forward potential. Applied Energy. 282:1-16. https://doi.org/10.1016/j.apenergy.2020.116135

Analysis of a novel concept of 2-stroke rod-less opposed pistons engine (2S-ROPE): testing, modelling, and forward potential

José Ramón Serrano Cruz[1], Francisco José Arnau[1]*, P. Bares and Alejandro Gomez-Vilanova[1]

J. Garrido-Requena[2], M.J. Luna-Blanca[2] and F.J. Contreras-Anguita[2]

(1) CMT Motores Térmicos, Universitat Politècnica de València, Spain
(2) INNengine

*Corresponding author: farnau@mot.upv.es. Telephone: (+34) 96 387 6500. Postal address: CMT Motores Térmicos. Universitat Politècnica de València. Camino de Vera s/n. 46022. Valencia. Spain.

Abstract

As pollutants and fuel consumption requirements become more constraining, new internal combustion engines generation arise to fulfill future automobile market regulations. In these context spark ignition (SI) engines working under hybridized structures are expected to represent one of the most viable and feasible technical approaches. In parallel to the already implemented 4-stroke turbocharged engines, new engine concepts are being conceived from their birth to meet nowadays standards. This work shows a new engine concept assessed to fit series hybrid configurations from the earliest design stages, and to fulfil requirements of the named "zero-emissions" urban areas. In this research work, a new opposed piston 2-stroke engine architecture based on rod-less innovative kinematics is described. The potential of this engine is based on its compactness, absence of vibrations and simplicity, going in hand with very competitive figures in terms of power density and fuel consumption. The engine unit has been designed, assembled, and tested to analyze several performance aspects, such as gas exchange and combustion. Taking advantage of the experimental campaign, a one-dimensional (1D) gas-dynamics engine model was developed and validated. Finally, the engine model was used for analyzing several potential upgrades and results have been discussed in detail. The target has always been to improve fuel consumption figures, below the best standards in market available internal combustion engines, while keeping engine concept simplicity and building costs.

Acronyms

A	Absolute pressure (bar)
AHR	Apparent heat release (J)
AHRR	Apparent heat release rate (J/CAD)
BDC	Bottom Dead Center
BSFC	Brake Specific Fuel Consumption (g/kWh)
CAD	Crank Angle Degree
CoV	Coefficient of Variation
cpm	Engine cycles per minute

DI	Direct Injection
BEV	Battery Electric Vehicle
G	Gauge pressure (bar)
HR	Heat Release (J)
HRR	Heat Release Rate (J/CAD)
IMEP	Indicated mean effective pressure (bar)
ISFC	Indicated Specific Fuel Consumption (g/kWh)
IVC	Intake Valve Closing
p	Static pressure (bar)
p0	Total pressure (bar)
PFI	Port fueled injection
Pmax	Maximum in-cylinder pressure (bar)
rpm	Revolutions per minute
R	Perfect gas constant (J/kgK)
SD	Standard Deviation
SE	Scavenge Efficiency
SI	Spark Ignition
T	Static Temperature (K)
T0	Total temperature
TE	Trapping Efficiency
TDC	Top Dead Center
TSI	Turbocharged Spark Ignition
VT&VCM	Variable Timing & Variable Compression Mechanism
1	Ambient conditions
2	Intake manifold conditions
2S-ROPE	2 Stroke Rod-less Opposed Pistons Engine
3	Turbine inlet conditions
3W	3 way (catalyst)
4	Turbine outlet conditions
ϕ	Equivalence ratio (fuel to air ratio divided by stoichiometric ratio)
λ	$\lambda=1/\phi$ Relative to stoichiometric air to fuel ratio

1. Introduction

Fuel economy and ultra-low-emission engines in urban areas are one of the main requirements to fulfill by engine manufacturers. In this context and after diesel-gate [1], new spark ignited (SI) engines are gaining attention in the automotive market research field. Two trends are found. On the one hand traditional SI 4-stroke engines are adapted to new regulations, researchers' efforts have resulted in: after-treatment studies [2], exhaust ports and turbine external insulation configurations [3] and cooled EGR with water injection technology [4]. Other studies attempt to modify the engine architecture such as three cylinder gasoline engine configurations [5] or exhaust manifold re-design [6]. Finally different combustion approaches [7] and pre-chamber ignition concepts [8] have also been studied. On the other hand, new engine concepts pursue accomplishing

the latest fuel consumption and emissions requirements [9]. Some innovative engine configurations are gasoline 2-stroke direct injection engines [10] and two stroke opposed piston engines [11]. It is this line where this study contributes with a new 2-stroke Rod-less Opposed Pistons Engine (2S-ROPE) concept.

One of the newest solutions motivated not only to reduce fuel consumption on SI engines, but also to minimize the ICE operation in urban conditions is the hybridization of the power unit [12]. The result is commonly known as Hybrid engine. Recent studies show potential advantages thanks to improved control methodologies [13] as well as synergies between both technologies have been deeply analyzed and computed in previous studies [14]. The potential avoidance of ICE usage in urban conditions by means of any hybridization technique, represents one of the most interesting solutions to pollutant emissions reduction in the urban areas. Moreover, it is in low load demand engine map area, where brake specific fuel consumption (BSFC) figures are more unfavorable, especially in SI engines, in which pumping losses represent a severe increase in BSFC (contrary to the diesels). In this line, it is of high interest the usage of batteries to recover energy from decelerations or directly from ICE, for later delivery [15]. What is more, problems of battery electric vehicle (BEV) are also mitigated by the usage of hybrid cars: in gross numbers, a BEV of about 400 km range would requires approximately 500 kg of batteries. With the same amount of rare earths for a single BEV, batteries for 40 hybrids can be manufactured. In other words, material collection issues [12] as well as batteries disposal ones, are much reduced.

The purpose of the study is to present a radically new engine prototype, which tries to achieve nowadays stringent BSFC and power demands from the very early stages instead of taking an already built basis which is re-adapted as normative changes. It is also the purpose of the paper to describe the main features with which the engine was conceived as well as to present the first experimental results, including combustion analysis. Finally, it is also pretended to show a prospective study by using an already calibrated 1D engine code, which contributes to the understanding of the engine behavior and main features. This final study shows potentially interesting areas from the BSFC, power demand and pollutant emissions perspective, and which may help in the next upgraded engine versions. The potentially obtained engine improvements by adding direct injection as well as working with lean mixture are assessed in this study and will constitute the basis for forward studies under different hybrid configurations. In global the work here described also shows a methodology, which combines a very first engine prototype with a short testing campaign and the setting-up of a purpose developed 1D gas-dynamic model. These three steps allow analyzing quickly and in a prospective study the major potentialities of the 2S-ROPE by calculation, and for further orientation of next prototypes and testing campaigns. In the section of the paper, where results of the modelling analysis are discussed, the main studied aspects are: the fuel injection (port or direct); the combustion (stoichiometric or lean combustion) and their corresponding turbocharging requirements. Aspects like the suitability of the intake and exhaust ports effective sections and the potential of the different injection and combustion concepts for the range extender purpose at 3000 rpm have been clearly stated.

The paper is structured as follows: Section 2 deals with a detailed explanation of the innovative engine architecture and how it is set up. In Section 3 the assembled unit is presented, as well as the experimental campaign and some combustion analysis. It is evidenced in Section 3 how experimental campaign and model development back up each other and help with the understanding of this engine working operation. Section 4 shows the results for different engine configurations, such as direct injection (DI), turbocharging or the potential of lean combustion if a combustion pre-chamber was taken advantage of. Finally, main conclusions are discussed in Section 5.

2. Engine description

This study deals with an innovative architecture of an internal combustion (IC) and spark ignition (SI) 2-stroke rod-less opposed pistons engine (2S-ROPE). This engine prototype has been patented, designed and manufactured by INNengine [16] and its range extender layout is known as e-REX [17]. It consists of a rotative mechanism based in a crank-shaft with faced cams perpendicular to the opposed pistons skirts (Figure 1). Bearings located at the skirts of the opposed pistons, rotate on the faced cams surface. The rotative movement of bearings at opposed cylinders skirts generate tangential forces on the border of the face to face cams of the crank-shaft. These tangential forces applied at a distance of the crank-shaft center generate torque and lie for alternative-to-rotative movement conversion (see Figure 1). 8 pistons are disposed in opposed pairs, sharing combustion chamber (see Figure 1_A), as well as intake and exhaust ports (see Figure 1_B). Randy. E. Herold et al.[18] have previously assessed some of the main thermodynamic benefits of opposed-piston 2-stroke engines. Among others, heat losses reduction and shortened combustions while preventing maximum rate of pressure rise constraints. But this is the first 2-stroke rod-less opposed piston engine (ROPE) described in the literature.

In Figure 1 DI configuration is shown, whilst the built prototype is a port fueled injection (PFI) concept. As it can be appreciated in Figure 1_A, one piston of each couple lies in the called “intake cam”, while at the same time, the other lies in the “exhaust cam”. Each complete “crank-shaft-with-cams” turn (which corresponds to an engine revolution) implies two entire cycles for all four cylinders. In all, eight complete cycles are achieved each engine turn. Figure 1_A shows how the cams are disposed: while in cylinders 1 and 3, pistons are at the Top Dead Center (TDC), the other two pairs of pistons are at the Bottom Dead Center (BDC).

Two exhaust lines are necessary to avoid cylinders interferences. This becomes a key point for gas exchange enhancement since 2-stroke engines do not include independent intake and exhaust strokes. Accordingly, cylinders 2 and 3 (in opposed phases), share exhaust line, as in Figure 1_C it is shown. This radically new engine concept is also equipped with a Variable Timing & Variable Compression Mechanism (VT&VCM). Due to the mechanism’s kinematics, a variation in terms of compression ratio also implies a given variation in terms of ports timing. In other words, an increase in compression ratio always implies and advance of exhaust port opening with respect to intake port opening, and one must take care and study the implications of this associated ports-timing variation. This mechanism offsets one of the rotary cams with respect the other.

Consequently, offsetting one of the cams does imply some displacement in the cylinders contacting the rotative cam. Reddish circular arrow in Figure 1_A shows how VT&VCM is actuated to select the desired position: exhaust cam is rotated several degrees with respect to the intake cam. The previous leads to the corresponding piston displacement (red straight row in Figure 1_A), with a number of collateral implications: cylinder volume, compression ratio and exhaust ports timing variations (since piston position determines all the previous). It was decided that exhaust cam was the only one with this freedom degree, while intake cam remains fixed. In all, when "exhaust cam" is offset, exhaust cylinders are displaced in axial direction (advanced or retarded taking as reference intake cylinders). Figure 1_D shows the different available VT&VCM positions: the exhaust port opening advance modification as well as the corresponding effective engine CR as a function of the actuator, which consists on a calibrated mechanism in which different linear positions correspond to different VT&VCM configurations. Figure 1_E shows both extreme VT&VCM positions and how available exhaust cylinder volume is offset in the engine cycle with VT&VCM actuation. Consequently, engine compression ratio is modified: as far as exhaust pistons are offset in axial position, total cylinder volume at intake valve closing (IVC) and BDC are modified. For better understanding, blue rows in Figure 1_E show how volumes at IVC have been modified according to the VT&VCM mechanism setup. The same happens with the volume at BDC. In all, as previously stated, engine CR is modified from values around 6.8 up to 9.5.

A value about 6.8 for the engine compression ratio (CR) may seem to be very low, especially taking into consideration nowadays standards and the direct impact of CR in the BSFC. In spite maximum CR is just 9.5, this is intentionally a derated engine with low maximum in-cylinder pressure to make easier achieving high reliability. Therefore, competitive figures of BSFC are pursued by lower heat losses (absence of cylinder head) and lower mechanical losses. The mechanical losses reduction is got by down-speeding, thanks to the 2-power strokes per cycle feature (lower rotating speed for the same power), the low maximum in-cylinder pressure itself and by the low number of moving components. Moreover, the authors of this work develop a zero-NOx proposal and study the viability of this engine configuration (as in section 4.2.3 about lean combustion is shown). For this purpose, it is necessary to provide the engine layout with compression ratio freedom and to widen CR values even below nowadays standards.

Also, it was decided to design the engine with a good range of variability for CR, so going down to CR=6.8 or up to CR=9.5 allows load control without throttling, what is very interesting to keep efficiency (low pumping losses) at low loads. As it will be shown in section 4.2.1, the VCR mechanism allows reducing load with respect to maximum CR up to 25% at 3500 rpm, which has been shown as maximum power engine speed. This last possibility of throttle-less load control has not been studied in this paper, in sake of brevity, and will be object of further works.

Furthermore, exhaust ports are closed or open according to exhaust piston movement. Hence, inherently and coupled to the engine mechanism, a modification in the exhaust piston position in the cycle leads to a variation in the exhaust ports timing. Figure 1_F

shows for both extreme mechanism positions, the exhaust port cross flow equivalent section.

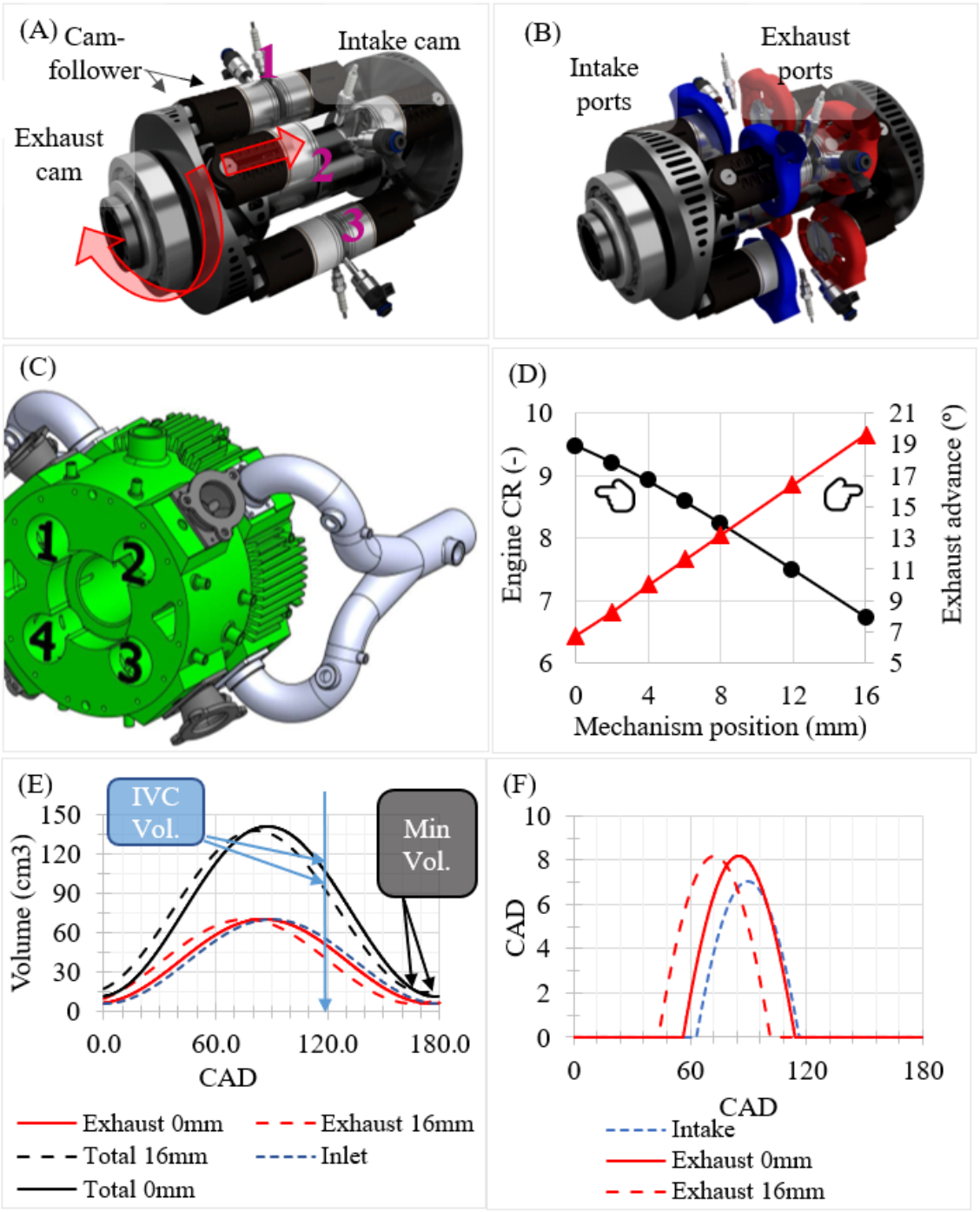

Figure 1: Engine configuration and VT&VCM examples. (A) Partially disassembled engine for easy schematic view. (B) Partially disassembled engine for easy schematic view of intake and exhaust ports. (C) Caption of external exhaust system and block. (D) Engine compression ratio and exhaust advance as a function of the mechanism position (mm). (E) Intake and exhaust cylinders volume as well as total volume variation with

CAD for 2 different mechanism positions. (F) Equivalent section for intake and exhaust ports as a function of CAD for different mechanism positions

One of the main reasons for the 2-stroke approach in combination with the two power strokes per turn and the 2 opposed pistons per cylinder is for mechanical losses reduction. They are achieved by means of avoiding low pressure loop (no pumping losses, but a scavenge pump is needed) and significant linear piston speed reduction (friction losses reduction). Figure 2_A shows for the 2S-ROPE, both: instantaneous and mean piston speed along 720º crank-angle degrees (CAD) (two complete engine turns that correspond to four complete engine cycles). The corresponding average engine rotative speed is of 1000 rpm, leading to 2000 cpm (cycles per minute) as it is indicated in Figure 2_A. Mean piston linear speed corresponds to 2 m/s and maximum to 3.1 m/s.

For reference purposes it is included the instantaneous and mean piston speed of a standard 4-stroke engine, with one piston per cylinder. The fact that a 4-stroke engine performs one complete cycle each 720º CAD, inherently implies four times the 2S-ROPE rotating speed if the number of cycles per minute is pretended to be kept (resulting in 4000 rpm for the same cpm). In addition, if one piston is in each cylinder, the complete stroke is to be covered by one piston, while in the 2S-ROPE, each piston covers half the stroke (half the linear velocity). Hence, typical 4-Stroke and one piston per cylinder engines, result in 4 times the rotative engine speed and 8 times piston linear speed for the same number of cpm, whilst contact points are divided by two with respect to the 2S-ROPE (as piston number is half than the 2S-ROPE). As previously stated, it is worth to insist that this analysis corresponds to one in which cpm are kept constant. The 4-stroke configuration would imply speed peaks around 25 m/s, while average linear piston speed is 16 m/s (8 times the 2S-ROPE piston speed).

If the same analysis is performed for a standard 2-stroke configuration (completing two cycles each 720º CAD or two engine turns), engine rotative speed is required to be two times the 2S-ROPE rotational speed. If one piston is inside each cylinder, the factor of two for piston linear speed calculation must be applied. Mean and maximum cylinder speeds are 8 m/s and 12.5 m/s, respectively.

In conclusion, the down-speeding proposal for the engine lies in the principle of minimizing sliding connections relative speeds, such as piston skirt to liner and segments to liner contact where most of friction losses are located [19]. Friction mean effective pressure (FMEP) is usually considered to vary with the square of the mean linear piston speed and other parameters such as load, oil temperature, camshaft, crankshaft, and segments technology. Assuming that load and working conditions are the same for all three previous cases (even 2S engines have no camshaft), equation (1) is evaluated for the, 4-stroke, 2-stroke and 2S-ROPE configurations.

$$FMEP_{cyl} = K \cdot {C_m}^{2\,\frac{N^{o}\,\frac{pistons}{cylinder}}{i}} \qquad (1)$$

Equation (1) is widely used for 2 and 4-stroke and one piston per cylinder engines [19], where K is a constant depending on load and lubrication conditions and "C_m" represents

mean piston linear speed. C_m is the term from which the 2S-ROPE configuration gets benefits. As previously discussed, piston speed is reduced as a consequence of half the stroke, hence the term" $N°_{pistons/cylinder}$" is necessary to take this into account. Finally, "i" considers the number of complete cycles per engine turn. Figure 2_B shows the results for the 2S-ROPE as well as for 2 and 4-stroke configurations. It is shown how FMEP is expected to be reduced in the 2S-ROPE configuration in comparison to the other two standard approaches.

It is worth noting that K coefficient from Equation (1) has been kept constant for 4S, 2S and 2S-ROPE. Nevertheless, the innovative kinematics based on a cam-follower mechanism with pure rolling contact (instead of sliding) joined to the lack of a cam-shaft and valve-train are expected to further reduce nowadays standard 4-strokes' K value for friction losses correlation. Another reason for 2S-ROPE configuration is mechanical vibration reduction: as far as the duty of the engine is to work and switch off alternatively as a function of battery level demand, the lower the engine vibration would result in higher passenger comfort without need of mass damping or mass mitigator addition. In all, start/stop maneuvers are expected to be less noticeable.

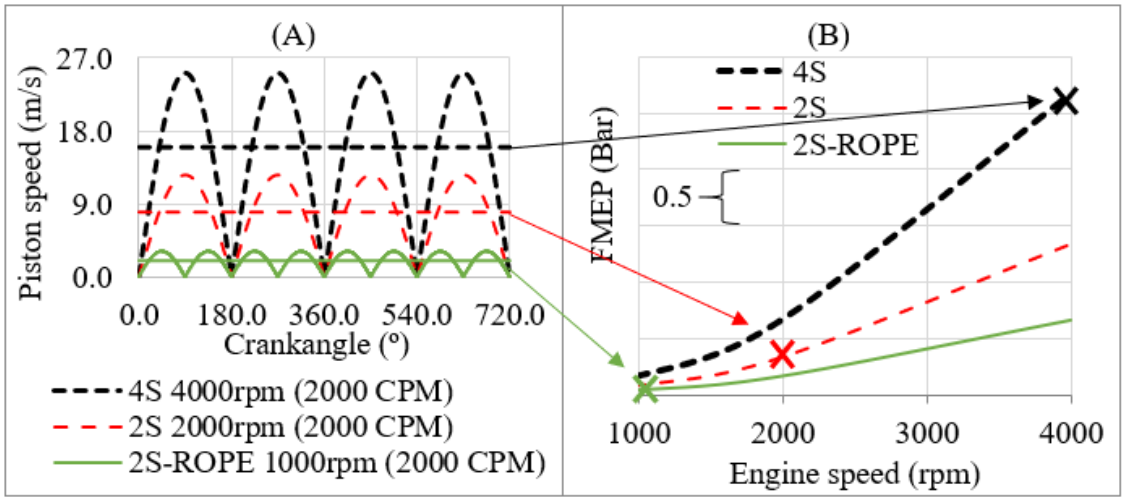

Figure 2: Pistons' instantaneous speed comparison between 4-stroke, 2-stroke and 2S-ROPE. (A) Instantaneous and mean piston speed for same cycles per minute, for different engine configurations. (B) Friction Mean Effective Pressure for the different engine configurations, as a function of engine speed. Crosses in (B) indicate que point in (A)

3. Experimental campaign and model validation

For the present work, the already described 2S-ROPE was manufactured, assembled (see Figure *3*) and tested at CMT-Motores Térmicos researching institute laboratories. The amount of data that was collected is low because of the limited prototype availability for the testing campaign and data acquisition. It is also worth to mention the fact that the testing campaign was not design for calibration or durability purposes. Testing was a preliminary check to analyze operativity, combustion and scavenging performance and with the purpose of calibrating models for further design objectives. It is also remarkable

the fact that since the engine control unit (ECU) was not yet calibrated for the engine, combustion and injection timing was controlled manually by the test cell engineers. Because of all the previous, and even though the engine was tested for approximately 150 hours, information available for the 1-D model calibration and validation is necessary contained. The 2S-ROPE was set up and stabilized in a reduced number of steady operation points but of high value for further model's calibration task.

Fuel was injected by means of port injection strategy in the tested unit, and tests were performed under a VT&VCM position corresponding to 2mm (see Figure *1*_B). This position corresponds to an engine compression ratio of about 9.15, while the exhaust opening advance it is of 8º CAD. Some main specifications are summarized in Table 1.

Figure 3: Final engine assembly and engine at test cell

Table 1: Engine description

Type of engine	S.I. 2-S ROPE
Number of pistons per cylinder	2 opposed pistons.
Displacement	500 cc each half engine revolution
Compression ratio	Variable, from 9.5-6.8
Number of cylinders	4
Type of injection	Port injection
Ports system	Variable exhaust timing
Intake boosting	Scavenge pump

One of the main targets of the experimental campaign was to analyze combustion process and verify that there is no misfiring in any cylinder while ensuring stable operating conditions. The heat evolution is obtained from the first and second thermodynamic laws:

$$mC_v dT = dQ - pdV \qquad (2)$$

which might be re-written if we assume ideal gas:

$$mRdT = m(C_p - C_v)dT = Vdp + pdV$$

and using the specific heat capacity ratio ($\gamma = C_p/C_v$) :

$$dQ = \frac{\gamma}{\gamma - 1} pdV + \frac{1}{\gamma - 1} Vdp \qquad (3)$$

where V is the instantaneous combustion chamber volume and p the in-cylinder pressure. The specific heat capacity ratio in a SI engine, i.e. where composition can be assumed stoichiometric and no EGR is expected, can be obtained as a function of the temperature, such as proposed by [20]:

$$\gamma = 1.38 - 0.2e^{\frac{900}{T}} \qquad (4)$$

where the temperature, $T(\alpha)$, can be computed from the pressure signal and the instantaneous volume evolution, by assuming ideal gas.

The evolution of heat in the combustion chamber (dQ) is meanly caused by the fuel combustion (HRR) and the wall heat transfer. Some authors suggest estimating the heat transfer by using semi-empirical correlations for modelling the convective coefficient (h), such as Woschni correlation [21]:

$$h = C_1 D^{-0.2} p^{0.8} T^{-0.53} [C_2 c + C_3 K(p - p_m)]^{0.8} \qquad (5)$$

where p_m is the motored pressure, c the average piston speed, C_1, C_2, and C_3 constants of the model, and K is obtained from the volume displace, V_{dis}, and the conditions at the Intake Valve closing (IVC):

$$K = \frac{V_{dis} T_{IVC}}{p_{IVC} p_{IVC}} \qquad (6)$$

Nevertheless, the coefficients must be obtained with a dedicated test campaign, and for a precise estimation, modelling other phenomena, such as blow-by, pistons deformation or friction losses, would be also required [22,23].

Another solution, to skip such intense testing campaign, and valid for a qualitative estimation of the combustion features is the apparent heat release. The apparent heat release is calculated using a constant polytropic coefficient (κ) instead of the specific heat capacity ratio (γ) to compensate the wall heat transfer and other phenomena. Apparent heat release is general practice at indication software when only indication is used for combustion control purposes [6]. A common value for κ is 1.3.

Figure 4_A shows the Apparent Heat Release (AHR) evolution for 30 consecutive cycles in a steady state working point for the cylinder 1 of the 2S-ROPE and for visual comparison purposes. For combustion stability analysis 150 cycles were processed. Figure 4_B shows the same information dealing with a similar working point in terms of engine speed and torque, but for a 4S Turbocharged Spark Ignited (TSI), Direct Injection

(DI) Engine. First thing that one can realize is the fact that effectively no misfires have been detected, the same was concluded for the whole 150 cycles batch.

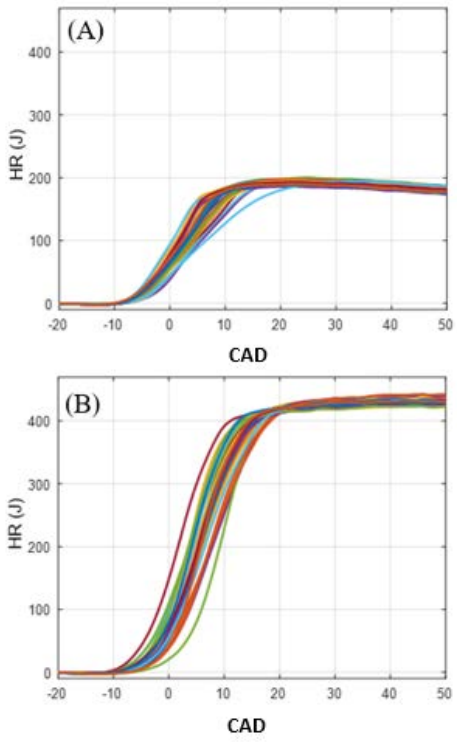

Figure 4: Combustion analysis of 30 cycles at 1000 rpm and 84 Nm. (A) 2S-ROPE. (B) 4S Turbocharged Spark Ignited (TSI) engine

The combustion efficiency (η_c) is calculated according to the equation (7), by comparing the ideal fuel energy capacity with the accumulated heat released.

$$\eta_c = \frac{\int_{SOC}^{EOC} HRR(\alpha)\ d\alpha}{m_f LHV} \qquad (7)$$

where m_f is the mass fuel burnt, LHV is the lower heating value (~46.4 MJ/Kg), and HRR is the heat release rate, which can be estimated from the in-cylinder pressure signal and the volume evolution as previously discussed. The start and end of the combustion, i.e. SOC and EOC, have been identified when a minimum value of heat release rate is obtained (a 3% of the maximum value at each cycle).

Table 2 summarizes the heat released obtained by using the apparent heat release and using Woschni correlation for modelling the wall heat transfer in both engines: in the 2s-ROPE and in the 4s TSI engine. Both engines were operated at similar conditions, 1000 rpm and 84 Nm (cycles shown in Figure 4). Results in the 2s-ROPE engine lead to a 60% combustion efficiency when using the apparent heat release and a 69% when including the wall heat transfer, while for the 4S-TSI-DI engine a 83% of apparent combustion efficiency was found and a 91% if Woschni approximation is used. The differences

between the actual combustion efficiency and the apparent combustion efficiency would depend on the operating conditions, as the apparent heat release method does not take into account the effect of the temperature in the wall heat transfer and in the specific heat capacity ratio. Note that other phenomena, such as blow-by or friction losses, have not been estimated.

It is found that there is an offset of 28 percentual points (in normalized terms) with respect to the TSI engine. This lack of efficiency it is explained by means of the short-circuit that takes place in 2S-ROPE at the analyzed point. However, to validate this hypothesis, it was necessary to validate the 1-D code.

Table 2 Combustion efficiency analysis: 1000rpm and 84 Nm working point

	HR [J]	AHR[J]	Fuel energy [J]
4s TSI, DI Engine	455.3	412.1	497.6
2S-ROPE	223.9	194.7	324.5

Figure 5 shows for the 2-S ROPE, for all four cylinders, the first 30 cycles apparent heat release rate (AHRR) in the same working point previously analyzed in Figure *4* and Table *2*. The bold black line corresponds to the average cycle. Figure *6* gathers the average cycle of each cylinder for combustion comparison. Analysis of Figure *5* and Figure *6* plots are summarized in Table 3, where CA10, CA50 and CA90 standard deviation (SD) in crank angle degrees terms and the coefficient of variation (CoV) of the maximum pressure and the IMEP are shown. Table 3 also includes for the 4S-TSI-DI the same combustion variability study. Although Figures only show 30 cycles for the sake of clearness, the average and the standard deviation were obtained by analyzing the complete set of tests, which were 150 cycles in the 2-SROPE and 300 in the TSI engine. SD and CoV are calculated according to equations (8).

$$SD = \sqrt{\frac{\sum_i^N (X_i - \bar{X})^2}{N}} \qquad CoV = \frac{SD}{\bar{X}} \tag{8}$$

where X_i corresponds to each of the CA10, CA50 and CA90 obtained, $\bar{X}$ corresponds to each studied variable average and N to the number of values considered. The variability in the CA10 is associated to variability at the ignition, while high variability at the CA90 is a signal of high dispersion in the combustion duration. Finally, CA50 variability indicates dispersion in ISFC and/or IMEP.

Cycle to cycle crank angle events SDs are very similar between both engine units. In fact, it is lower in the 2S-ROPE engine at CA10 and CA50. However, CA90 SD and maximum pressure CoV are much higher what ultimately explain the higher IMEP CoV of the 2S ROPE. Cycle to cycle variation is calculated according to the standard deviation, taking for all the cycles shown, the CA10, CA50, CA90, Pmax and IMEP. In terms of cylinder to cylinder, dispersion is calculated as the standard deviation of the average cycles shown in Figure 6. In comparison to the 4S-TSI-DI reference engine, it was found a considerable

deviation between cylinders in all analyzed variables. Maybe due to lack of uniformity in the cooling system or cylinder to cylinder casting and manufacturing dispersion in the prototype since the intake and exhaust system were perfectly symmetrical. Forward and wider operative combustion analysis would be required in future stages. Table 3 shows how for the 2S-ROPE CA90, 6.4º crank angle degrees variation between cylinders is expected, and about 50% higher CoV in maximum pressure. Both finally causes 5 times higher CoV in the 2S-ROPE than in the standard 4S TSI engine.

Tested working points as the one for which combustion analysis has been described, where intentionally dealing with relatively low engine speed and torque. Torque was kept below 50% load; the purpose was to ensure the engine integrity before the visual wear inspection, which would allow for later experimental campaigns covering a wider range of engine torque and speed. Even if low torque was desired to be reached, specific obtained torque figures were the result of the spark advance manually set up at the test cell (since no ECU was already calibrated). Low speed also generates lower swirl and turbulence intensity inside the combustion chamber what is especially critical when combustion stability wants to be assessed.

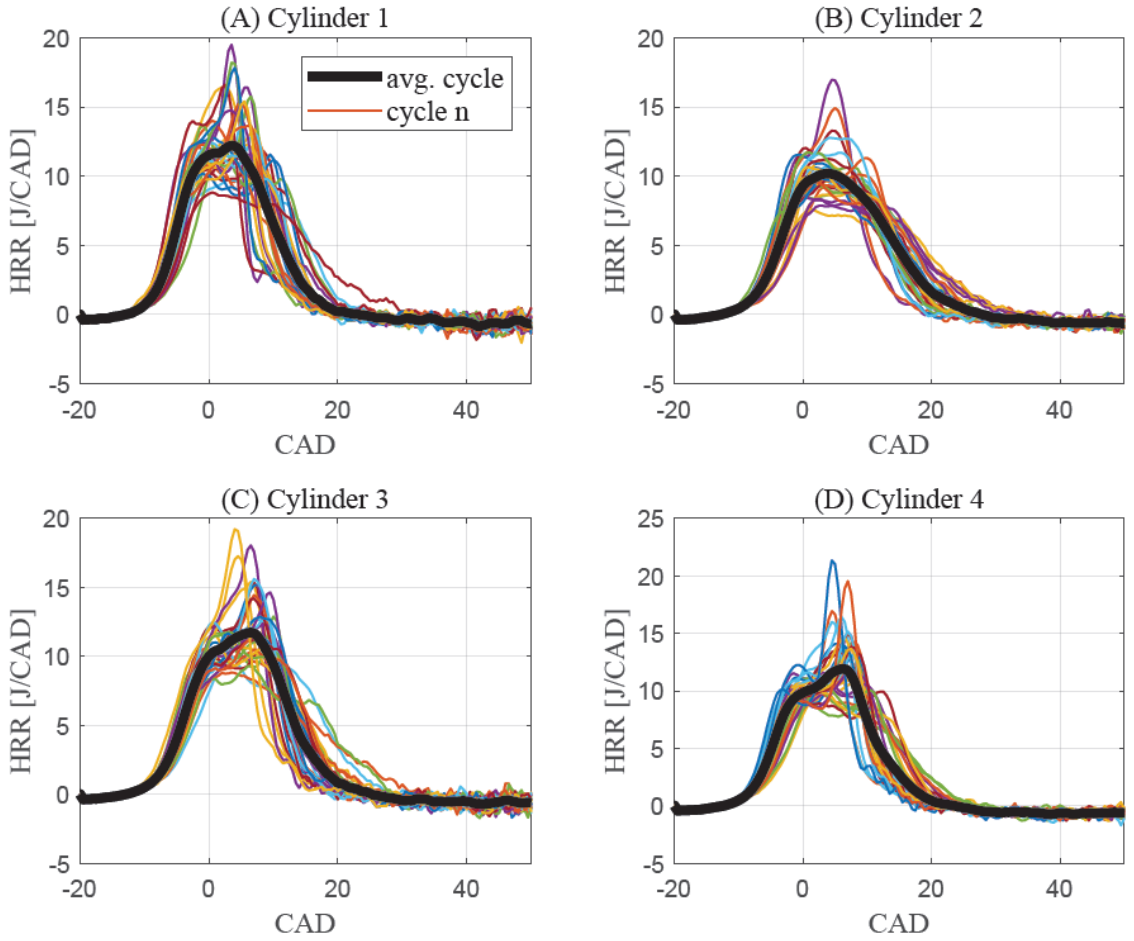

Figure 5: HRR for cylinders 1-4 at 1000 rpm and 84 Nm. Average and first 30 cycles. (A) Cylinder 1. (B) Cylinder 2. (C) Cylinder 3. (D) Cylinder 4

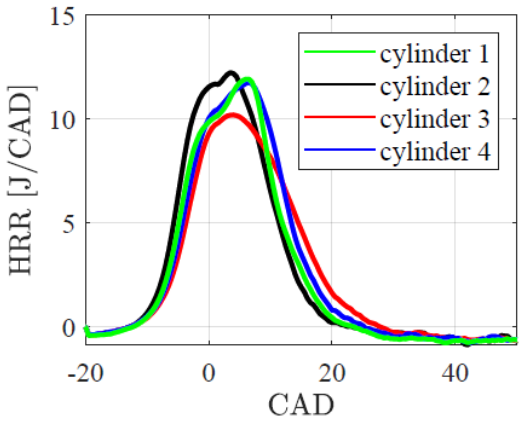

Figure 6: HRR for cylinders 1-4 at 1000 rpm and 84 Nm

Table 3: Standard deviation of combustion parameters and coefficient of variation of in-cylinder variables. 1000rpm and 84 Nm working point.

		CA10	CA50	CA90	Pmax	IMEP
			SD (cad)		CoV (%)	CoV (%)
cycle-to-cycle variability	4s TSI, DI Engine	1.2	1.6	2.1	5.76	0.88
	2S-ROPE	0.8	1.5	3.2	11.53	3.62
cylinder-to-cylinder variability	4s TSI, DI Engine	0.8	1.1	1.7	5.67	0.93
	2S-ROPE	1.7	3	6.4	8.89	4.53

4. Modeling activities

Engine modelling activities have been performed with in-house developed software called VEMOD [24], in which the special architecture and kinematics of 2S-ROPE has been programmed. VEMOD is a 1-D gas-dynamics code for engines and thermo-fluid systems simulation. In this section first will be validated the engine modelling in terms of kinematics, and gas exchange process, further prospective studies are done to evaluate engine potential in terms of power and ISFC. In the cases discussed along this section, both intake and exhaust ends are connected to an environment with imposed and fixed atmospheric pressure. Inlet pressure is also imposed to be the desired one for each simulation. Hence, no turbocharger or boosting unit are implemented in the simulations. In this study main potential operative regions are to be identified and evaluated for later boosting technique selection discussion as a function of working conditions.

4.1 Gas-dynamic model validation

Figure 7 allows validating the model compression ratio, kinematics, combustion, and gas exchange modelling using the perfect mixture hypothesis. This figure deals with the instantaneous experimental data of the 1000 rpm and 84 Nm working point analyzed in

previous section from combustion perspective. The experimental information is compared against the instantaneous pressure evolution prediction. Figure 7_A deals with cylinder pressure evolution during the complete cycle. Figure 7_B, Figure 7_C and Figure 7_D show instantaneous pressure evolution during the gas exchange process. The high degree of agreement allows to validate the model mass flow predictions, including short-circuit among other phenomena.

Figure 8 highlights for the 1000 rpm and 84 Nm working point how the 1-D model predicts the short-circuit. Figure 8_A deals with instantaneous mass flow through intake and exhaust ports. Positive intake mass flow corresponds to a net flux going into the cylinder, negative exhaust mass flow, means that there is flow leaving the cylinder. As it can be appreciated, after the exhaust blowdown takes place, then fresh air goes into the cylinder (highlighted area 1). See how cylinder trapped composition varies accordingly in Figure 8_B for highlighted area 1. To understand what follows, it is a key point to clarify that the information shown in Figure 8_A and Figure 8_B corresponds to a simulation performed under perfect displacement model approach: fresh air displaces the burned gases and there is no short-circuit until the last molecule of burned gas leaves the discretized volume. This is the most desirable solution since there would be no short-circuit until all the burned gases leave the cylinder. It is shown that no residuals remain in the cylinder in the highlighted area 2 of Figure 8_B. However, moving back to Figure 8_A, one can see that as a given air mass flow enters into the cylinder through the intake ports, it also leaves it almost simultaneously through the exhaust ports. As far as there are not exhaust gasses left, short-circuit is taking place.

On the contrary, in the perfect mixture approach, a perfect mixture is produced in the cylinder each time-step, and it is the mixture what is considered to leave the cylinder. Perfect mixture results are disposed in Figure *8*_C and Figure *8*_D. In highlighted area 2 as fresh air goes into the cylinder through the intake ports, a perfect mixture leaves the cylinder (in all, short-circuit). This is why in Figure *8*_D, area 2, during ports opening overlap, while there is still burned gas present, fresh mixture enters into the cylinder and partially leaves. In all, the previous results in short-circuit and some residuals trapped for the next cycle (highlighted area 3). For the analyzed point there is a 45% of short-circuit, in the perfect mixture approach, while a 39% happens in the perfect displacement approach.

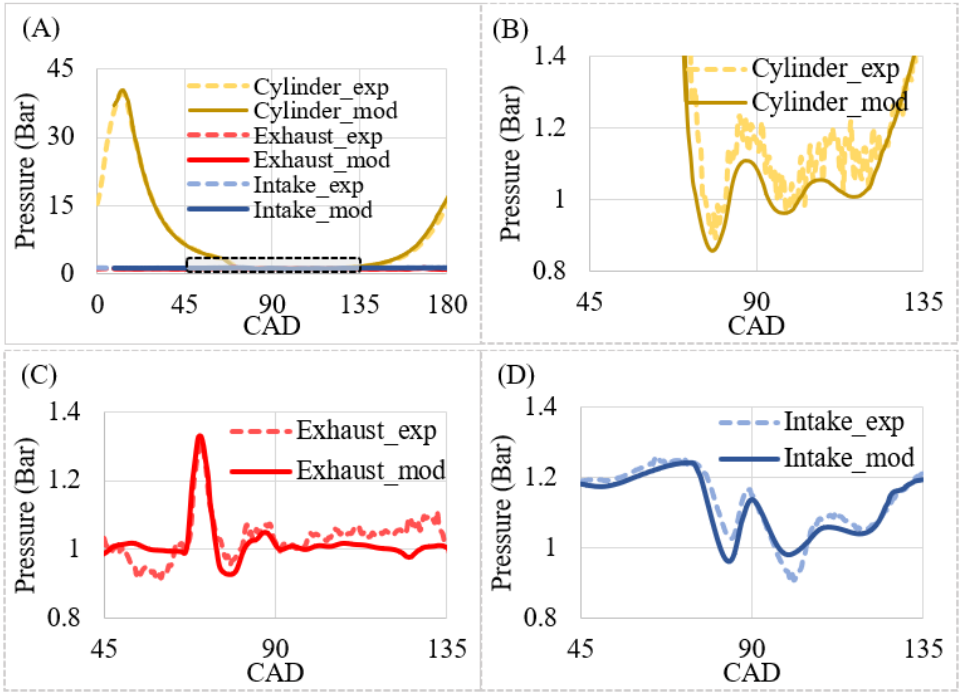

Figure 7: 1000 rpm/84 Nm model and experimental instantaneous pressure evolution. Perfect mixture approach. (A) Gathers cylinder, exhaust and intake model and experimental pressures. (B) For detail evolution of cylinder pressure during valve gas exchange. (C) For detail evolution of exhaust pressure during gas exchange. (D) For detail evolution of intake pressure during gas exchange.

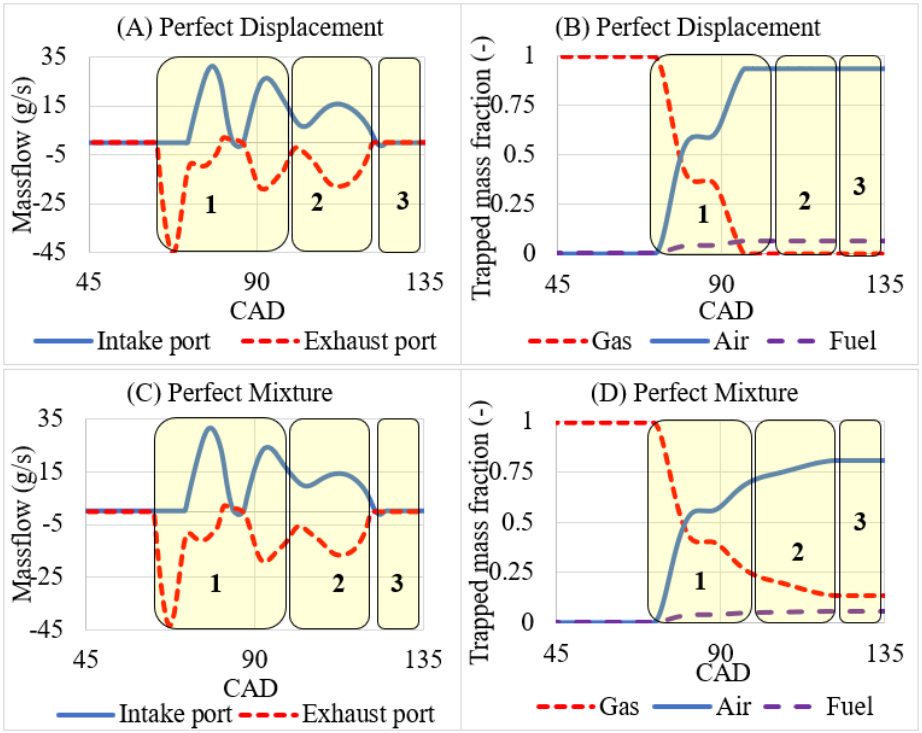

Figure 8: 1000 rpm/84 Nm model. (A) Mass flows with perfect displacement. (B) Instantaneous composition variation with perfect displacement. (C) Mass flows with perfect mixture. (D) Instantaneous composition variation with perfect mixture.

Finally, also for validation purposes, several experimental working points have been compared against the obtained “engine maps”. Figure *9* shows for air mass flow and torque, the experimental and model agreement. Figure *9*_B and Figure *9*_D deal with indicated experimental torque instead of brake torque because of the lack of knowledge about a mechanical losses model predictable enough for this novel engine configuration. The indicated torque was experimentally obtained at every engine speed as the addition of combustion brake torque plus motoring brake torque. Therefore, mechanical losses were experimentally estimated as the brake torque during motoring conditions at the same engine speed. The engine auxiliars (oil pump, water pump and scavenge pump) were excluded from the friction losses since they were not powered by engine crank shaft but from engine external power sources supplied by the test cell. That is why mechanical losses value have not been reported in this work and will be studied after auxiliars will be defined and moved by the engine. The procedure to locate the experimental points in the obtained predicted maps it is by fixing in the maps both: the engine rpms and the inlet pressure (p02) from the experimental campaign. The point where both lines match, correspond to the operative point (dotted red lines in Figure *9*). Text in boxes corresponds to the experimental collected data (stars), while figures discretizing iso-magnitude working ranges correspond to model predictions.

Both gas exchange approaches are considered for the validation stage: Perfect mixture and displacement. In terms of air mass flow, differences are almost negligible (see Figure *9*_A and Figure *9*_B). The perfect displacement model overpredicts torque output in higher degree below 2000 rpm. On the contrary, perfect mixture results fitted better to the experimental campaign. However, from 2000 rpm in advance, better results were obtained under perfect displacement approach. Further studies are needed for calibrating a trapping and scavenging efficiency model for the 1D gas-dynamic model. At this stage, the behavior is as expected in standard 2S engines.

Air mass flow discrepancies may be attributed to volumetric efficiency differences due to heat transfer miss prediction (standard Annand model was used) and differences in the backflows and instantaneous scavenge performance calculation. Regarding torque, errors are mainly attributed to combustion cycle-to-cycle variability (the mode of 30 cycles were used as apparent heat release law), heat transfer calculation errors and possible uncertainties when the conversion from experimental brake torque to experimental indicated torque was done. For example, since motoring test were taken as a first approximation for mechanical losses estimation, in-cylinder pressure differences with respect to actual combustion conditions were neglected, but this term also influences this type of losses. However, with the relatively reduced amount of data at this development stage, model predictability is considered worth for further analysis and by model design studies.

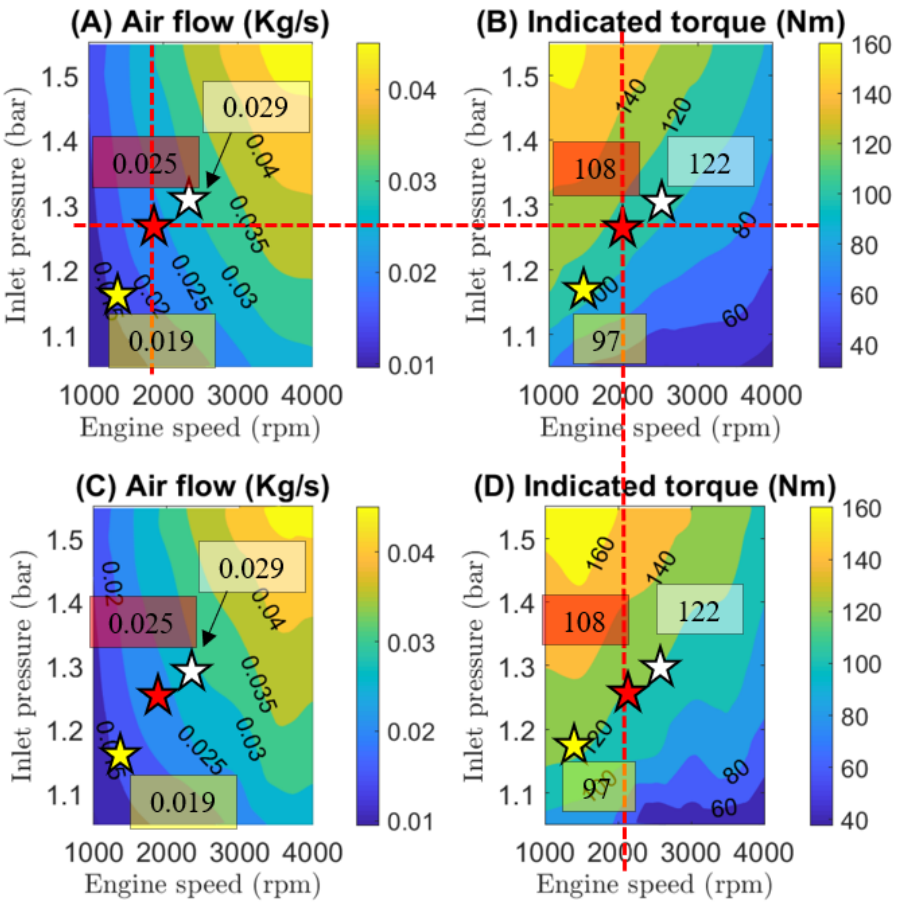

Figure 9: Model validation in terms of air mass flow and indicated engine torque. Experimental information are stars and contours represent the calculated maps. (A) Air mass flows with perfect mixture. (B) Torque with perfect mixture. (C) Air mass flows with perfect displacement. (D) Torque with perfect displacement

4.2 Prospective studies and 1-D gas-dynamics model results discussion.

After having checked instantaneous data for kinematics and timing, as well as mean variables such as air mass flow and torque, authors have performed some prospective analysis using the 1D engine model. In other words, taking advantage of the purposely developed engine model, it is possible to perform design by simulation at early prototype phases. These studies are done to identify the most interesting operative areas from: emissions, BSFC and power perspectives. One of the main motivations when developing such 1-D models is the flexibility to explore engine configurations or injection strategies, while keeping the main engine design parameters well modelled.

Three main engine configurations have been analyzed: scavenge pump with port injection (corresponding to the already built engine prototype), turbocharged direct injection, and turbocharged direct injection combined with lean combustion. Turbocharger is not considered to be assembled in the port injection option since high simplicity and low cost are desired and therefore number of components to be as low as possible in this configuration. Hence, boost pressure is obtained just by means of a simply controlled scavenge pump that would imply extra mechanical losses. For the other two

configurations, turbocharging is assessed to find the most efficient solution, assuming the potential cost increase.

Despite the engine behaves closer to a perfect mixture in low speed operative conditions, in this section simulations have been performed under perfect displacement approach. The reasons are twofold, the series hybrid use of this engine will take place at high speeds (about 3000 rpm) and the study is aiming to evaluate the best reachable situation. The target is to identify the potential working areas for later ports re-design, pursuing a perfect displacement gas exchange in the desired working conditions. Variables are shown in indicated terms, as far as mechanical losses are still not modelled and there is very little information about the influence of speed and cylinder pressure on friction losses. In any case and whatever configuration selected, the main purpose is to identify the most efficient areas that may potentially fit with both: power requirements and available aftertreatment technologies. It is worth noting again that the final application of this engine in this paper is for a series hybrid configuration for automotive transport purposes. The engine final duty is to charge a set of batteries, disposed in a series configuration with the e-REX version of INNengine 2S-ROPE. This way, engine operation is to be restricted to the design area. Figure 10 is an example of series hybrid working scheme in which the direct drive engine charges the batteries, whilst the electric motor powers the car.

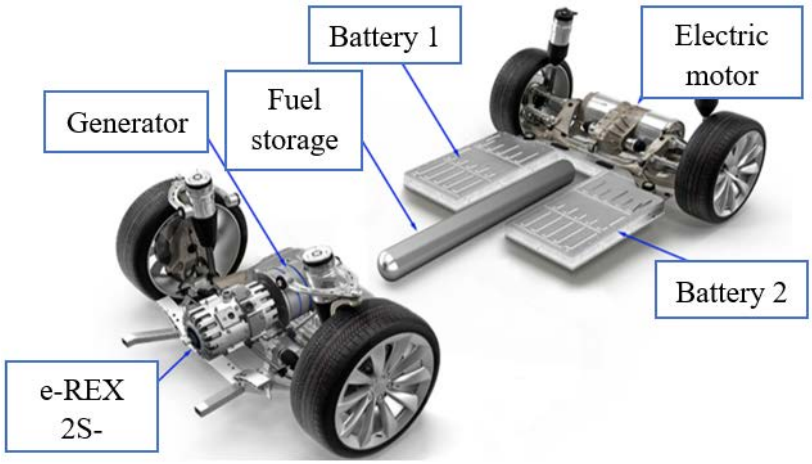

Figure 10: e-REX version of INNengine 2S-ROPE coupled to batteries and an electric motor for series hybrid configuration (range extender). Design proposal

4.2.1 Port injection

The main issue to be considered under this configuration it is the short-circuit. Even if perfect displacement approach is adopted for the complete set of simulations, some short-circuit and residuals in the cylinder are inevitable along the major part of the engine operation area. To evaluate the engine most desirable operative areas, some coefficients definitions are necessary to be considered. Scavenge efficiency is defined in equation (9), and trapping efficiency in equation (10). These are some of the parameters that evaluate gas exchange performance in two stroke engines [25]. Figure 11 shows the terms that are considered in equations (9) and (10) in a more schematic view. Scavenge efficiency gives information about the ratio of residuals in comparison to the total amount of trapped gasses: a value of one indicates that there are no residuals, a value of zero means that all

the combustion chamber if filled with purely burned gasses. Trapping efficiency deals with the ratio of fresh mass retained for next cycle power delivery, with respect to the total fresh air being inducted by the engine. A value of one means that all the fresh air is trapped (zero short-circuited mass), the lower the value the higher short circuit.

$$SE = \frac{\sum_{i=1}^{n-cylinder} m_{retained}}{\sum_{i=1}^{n-cylinder} m_{trapped}} \quad (9)$$

$$TE = \frac{\sum_{i=1}^{n-cylinder} m_{retained}}{\sum_{i=1}^{n-cylinder} \oint \dot{m}_{inlet}} \quad (10)$$

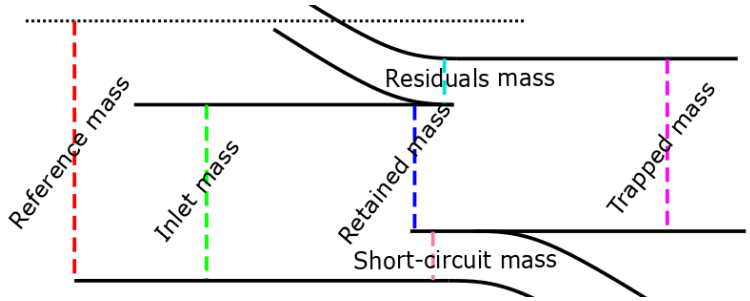

Figure 11: Flow diagram for scavenging parameters definition

As previously said, simplicity and costs are some of the main targets in this engine configuration. A mechanical compressor providing with a slight boosting of 150 mbar(G) is assumed. By 150 mbar(G) it is intended that the boost pressure is 150 mbar above the reference pressure which is the atmospheric pressure (1 bar). Hereinafter (G) refers gauge pressure and (A) refers absolute pressure. To study the effect of the VT&VCM, a specific modelling campaign dealing with the freedom degree of the VT&VCM has been performed. Figure 12 shows for the range of 1000-4000 rpm and a fixed boost pressure of 1.15 bar(A). Trapping and scavenging efficiencies (Figure 12_A and Figure 12_B), power (Figure 12_C) and ISFC (Figure 12_D) are shown. It is concluded that for whatever VT&VCM position, short-circuit is only avoided in the 3000-4000 rpm range. It is also concluded that the operative area around an engine CR of 8.5 to 9.2 is the most optimum one: thanks to the higher CR and to the higher SE. See how the influence of the SE evolution impacts power and ISFC trends (black dotted rows).

The main advantage of this configuration is the simplicity and lightweight resulting combination. Aftertreatment requirements consist only of a 3-way catalyst, while injection system is very simple, cheap, and reliable. The required boost pressure could be easily achieved by means of an external mechanical compressor.

Additionally, the VT&VCM system could be consider an option for load control at constant speed. If one analyzes indicated power (Figure 12_C) at 3500 rpm, where a maximum power value of 32 kW is obtained, the VT&VCM system allows a load control

that ranges between 32 kW and 24 kW, this is a 25% load control capability without throttling and keeping a ISFC quite constant and around 250 g/kWh.

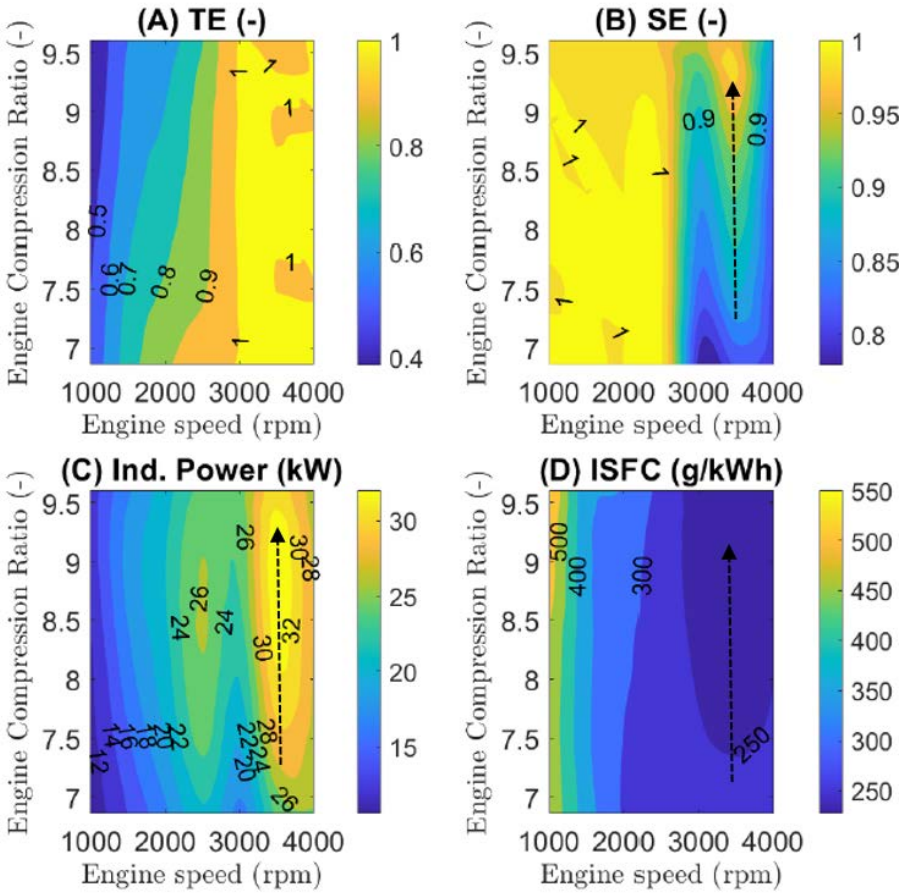

Figure 12: Simulations results for port-injection configuration (boost pressure of 1.15). Maps for the different variables as a function of the actuator position and engine speed. (A) Shows trapping efficiency. (B) Shows scavenge efficiency. (C) Shows indicated power. (D) Shows indicated brake fuel consumption

4.2.2 Direct injection

By implementing direct injection, fuel short-circuit is avoided. Hence, trapping ratio is not a limiting parameter, from fuel short-circuit and efficiency perspective, anymore. In addition, it could be considered a turbocharger implementation, what would result in a more efficient solution since exhaust gas energy can be partially recovered, what goes in hand with a reduction for the scavenge pump work. However, DI & turbocharging would imply a more expensive and complex solution.

Simulations were performed with a direct injection configuration. Fixed VT&VCM mechanism position was set-up at 9.2 CR value and for a p02/p03 ratio swept going from 1.05 to 1.55 and simulating turbocharger boost pressure. In this configuration is considered that the boosting (p02) needed for scavenging duty is helped by a turbocharger unit, hence, a given backpressure to the engine is built by the turbine (p03) in order to expand hot exhaust gases. Thanks to exhaust gases expansion, boost pressure is also built,

in all a p02/p03 is obtained. It is worth noting, that for a 2S engine, such as the one in this study, a positive pressure gradient is always required for a proper scavenge process.

Figure 13 shows results from the simulations. First of all, circled area in Figure 13_A corresponds to the area that would be closer to power requirements (above 30 kW). ISFC values are in the range of 205-215 g/kWh (see Figure 13_B). This implies a 45-35 g/kWh improvement in comparison to the 250 g/kWh of the optimum port injection operative area. In fact, the engine range of usage under DI configuration is considerably improved in both dimensions, boost pressure and engine speed, since it is not compulsory to work at 3000 engine rpms to fit the power demand (just convenient in order to avoid the gear box between the 2S-ROPE and the electric generator). Also, it implies BSFC advantage, since boosting architecture can be upgraded with the turbocharger and scavenge pump power consumption can be highly reduced. The main issue in this configuration are NOx emissions. Figure 13_C reveals that 2500 ºC are easily reachable. The usage of a three way (3W) catalyst is then compulsory and only possible if trapping efficiency is one (Figure 13_D). Otherwise, short-circuited oxygen would not allow reducing NOx in a 3W catalyst. It is then concluded that only shaded operative areas named as "1" and "2" are compatible with a 3W catalyst. The ISFC in these working areas corresponds to approximately 216-220 g/kWh.

Exhaust temperatures in both shaded areas are quite high (Figure 13_E). This is intimately related to the zero fresh air short-circuit. What is more, exhaust gas temperature is around the optimum for turbocharging purposes: around 900 ºC. Nowadays radial turbines for ICE applications can withstand 950 ºC approximately. The closer to the maximum allowed temperature, the lower the backpressure requirements for a given intake/exhaust pressure ratio. Required p02/p03 is around 1.35 and 1.21 for areas 1 and 2, respectively. These pressure ratios feasibility is evaluated by means of equation (11), through which it can be calculated the required turbocharger efficiency for a given boost pressure, depending on the turbocharger working conditions or the desired boost level.

$$\eta_{tbc} = \left(\left(\frac{p_{02}}{p_{01}}\right)^{\frac{\gamma_c - 1}{\gamma_c}} - 1\right)\frac{Cp_c}{Cp_t}\frac{T_{03}}{T_{01}}(1 + \phi)\left(1 - \left(\frac{p_4}{p_{03}}\right)^{\frac{\gamma_t - 1}{\gamma_t}}\right)^{-1} \qquad (11)$$

- Compressor inlet pressure ($\boldsymbol{p_{01}}$) is obtained from experimental data coming from the reference 4S DI-SI engine whose HR was shown in Figure 4. A first $\boldsymbol{p_{01}}$ estimation was made taking a working point with similar air mass flow to the one in the 2S-ROPE for the selected area of interest. The same is performed for $\boldsymbol{p_4}$. The last is of great importance to be realistic in terms of pressure losses imposed by nowadays DI SI after-treatment systems, for the mas flow range in question.
- $\boldsymbol{Cp_c}$, $\boldsymbol{Cp_t}$, $\boldsymbol{\gamma_c}$, $\boldsymbol{\gamma_t}$ correspond to specific heat capacity and heat capacity ratio of fresh air and exhaust gases, respectively. Sub-index "c" corresponds to compressor while sub-index "t" to turbine.
- Turbine inlet pressure ($\boldsymbol{p_{03}}$) corresponds to a parametric variable within the range of 1.1 to 3.0 bar(A).

- Exhaust temperature ($\boldsymbol{T_{03}}$) it is taken from the 2S-ROPE simulations in the selected area, which corresponds to 900 ºC.
- $\boldsymbol{p_{02}}$ corresponds to compressor outlet pressure, and it is imposed to be 1.21 or 1.35 times $\boldsymbol{p_{03}}$, as far as simulations suggested that this corresponds to the most favorable working range.
- Finally, ϕ corresponds to the equivalence ratio.
- Turbocharger efficiency ($\eta_{\boldsymbol{tbc}}$) is the product of turbine times compressor times bearing system mechanical efficiencies as defined in equation (12). It is the unknown that informs about the realistic/unrealistic attempted boosting level, for the given boundaries (such as $\boldsymbol{T_{03}}$, the desired $\boldsymbol{p_{02}}$, the generated $\boldsymbol{p_{03}}$ ...). Authors' experience and collected data in the field suggests that 40% would be a realistic approximation of nowadays maximum turbocharger efficiency [26].

$$\eta_{tbc} = \eta_{turbine}\,\eta_{compressor}\,\eta_{mechanic} \qquad (12)$$

The resulting continuous blue and orange trends in Figure 14 show for both p02/p03 levels (1.21 and 1.35), the required turbocharger efficiency obtained from equation (11), for the 2S-ROPE, as a function of the p03/p4. The higher the turbine pressure ratio (p03/p4), the lower the required turbocharger efficiency.

Figure 14 also shows in dashed blue and orange (for both p02/p03 levels of 1.21 and 1.35 respectively) the compressor pressure ratio that results for each p03/p4. In other words, the higher p03 the higher p02 to guarantee the desired p02/p03. This information is referred to the secondary axis. The T03/T01 values used to plot this chart are 1173 K / 293 K according to Figure 13_E data.

For reference and double check purposes, point A (2500 rpm and 280Nm) dealing with experimental information from the reference 4S-TSI-DI engine has been included in the plot. Point A deals with a T03 value of 910 ºC and a p02/p03 ratio of 1.15. The turbocharger efficiency is around 39 %. Continuous grey line corresponds to the efficiency trend predicted by equation (11) to accomplish the aforementioned p02/p03 ratio and it fits the experimental point A perfectly. As previously stated, p02/p03 of point A is about 1.15, while it is included in the orange dashed trend, corresponding to 1.35 of p02/p03. This happens because the air mass flow in the experimental point A, for the 4S-TSI-DI engine is considerably higher, leading to a higher p4. Hence, when plotting p02/p01 as a function of p03/p4, even if p02/p03 is lower, the much higher p4 offsets point A to the left, as the p03/p4 is diminished by the p4 influence.

As for the experimental working point, if a turbocharger efficiency of 40% is expected for the 2S-ROPE (black continuous bold horizontal line), resulting turbine pressure ratio would be of 1.80 and 1.35 for both selected p02/p03 (1.35 and 1.21 respectively). Crosses indicate the intersection between 40% efficiency and predicted efficiency trends for both p02/p03, according to equation (11). Colored vertical continuous arrows indicate p03/p4 value for a 40% of turbocharger efficiency. For the corresponding p03/p4, compressor pressure ratio is indicated with dashed colored horizontal arrows.

In all, the p02/p03 of 1.35 is in the limit of what could be achieved, as it is almost overlapped with nowadays available turbocharger technologies. For the p02/p03 of 1.21, no problems are expected to get needed turbocharger efficiency. It can be concluded a limited need of scavenge pump usage in the operative range (limited to engine cold start and similar operations) what points to a good mechanical efficiency and promising figures of BSFC. In addition, there is some “margin” in case that boundary conditions were further unfavorable, such as altitude. By generating a slightly higher p3 (with a variable geometry turbine for example), the effect of altitude for the p02/p03 achievement could be fixed (up to a certain point).

The main drawback is engine speed range for which all the previous is stated: 3000 to 4000 rpm. This means that from the friction losses point of view, it is not the most efficient operative area. However the mechanical losses expected would be in the order of magnitude of a 4-stroke engine operating around 2000 rpm (see Figure 2). It is clearly evidenced how this downspeeding approach for friction losses reduction, by means of a 2S high power density cycle with opposed pistons, would help to improve BSFC figures. Finally, is worth noting that the gas exchange process of the 2S-ROPE cycle is the main reason why engine operative area dramatically reduces. However, for a series hybrid application, with a single operative working point, the main drawback is neglected while engine simplicity and efficiency figures are highly competitive. It is also evidenced that the main issue in the direct injection configuration are NOx emissions, and how aftertreatment determines the operative area of the engine for a series hybrid configuration.

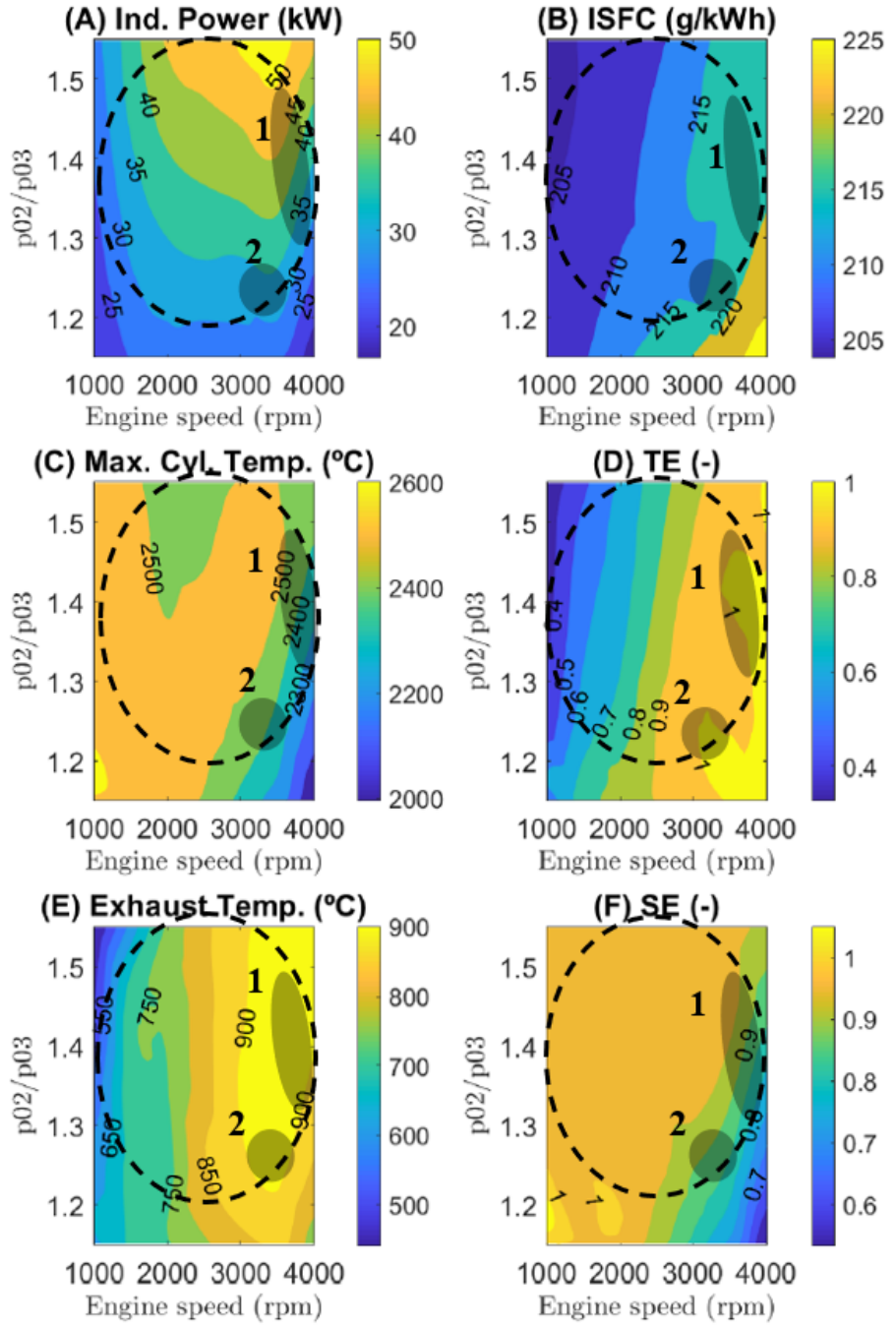

Figure 13: Direct injection simulation results. Engine CR=9.2 (2mm VT&VCM position). Different variables evolution as a function of the p02/p03 and engine speed. (A) Shows indicated power. (B) Shows indicated brake fuel consumption. (C) Shows maximum cylinder temperature. (D) Shows trapping efficiency. (E) Shows exhaust temperature. (F) Shows scavenge efficiency

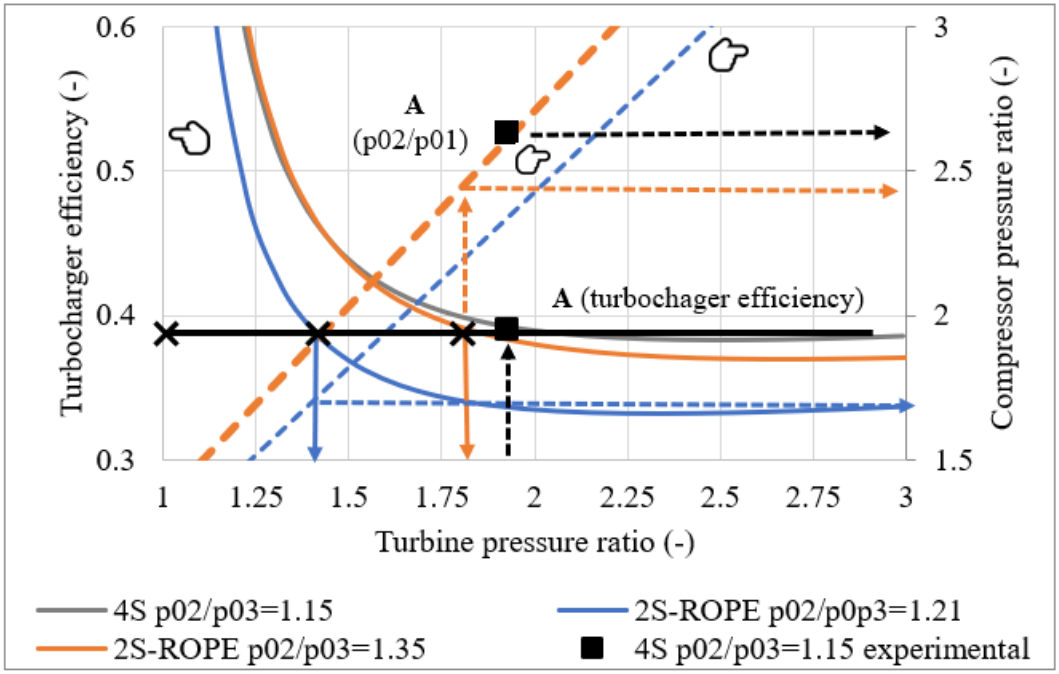

Figure 14: Turbocharger efficiency and resulting boost pressure for different exhaust pressure values. Point B from 4-stroke turbocharged SI modern engine for reference. 2S-rope T03/T01=1173/293

4.2.3 Lean combustion

Because of previous studies, authors have assessed the impact that a leaner mixture has in terms of maximum cylinder temperature. Maximum cylinder temperature it is not the maximum temperature obtained in the flame (where NOx emissions are generated) while it progresses through the combustion chamber. However, trends have been obtained and provide with a good estimation about ϕ required to diminish maximum cylinder temperature to 1925 ºC [27]. The motivation of this idea it is to assess the equivalence ratio ($\lambda=1/\phi$) range required to avoid high enough temperatures for NOx generation. This way with the usage of an oxidation catalyst for HC, CO and other partially unburned species could be enough for emissions requirements since the engine would be with zero NOx emissions before the aftertreatment. Hence a simpler and cheaper after-treatment would potentially result, while efficiency improvement is also evaluated.

The usage of combustion pre-chambers looking for the commonly known as torch ignition phenomena results of high interest for complete and repetitive highly diluted combustions. Some studies dealing with combustion pre-chambers show values for the relative AFR (λ) of $\lambda=1.73$ [28]. Among other advantages of pre-chamber systems it shortens combustion time, reduces combustion variability and enlarges the knock limit [29]. As far as the engine operation as range extender is supposed to reduce dramatically in comparison to nowadays ICE, it could be feasible to calibrate and design a combustion pre-chamber for the e-REX 2S-ROPE concept (Figure 1 and Figure 10).

An iterative loop was carried out to solve the following optimization problem: to find the λ that provides with an operative area where the maximum cylinder temperature is around 1925 ºC, whilst that working area provides with 30 kW or more. Several areas or configurations have been obtained, but another requirement was considered: exhaust temperature. Boosting the engine up to the values predicted by the simulation can be done by means of a turbocharger plus a scavenge pump, the higher the exhaust temperature the easier to accomplish boosting targets. As a first rough estimation, 700 ºC are a must if a turbocharger is aimed to be coupled and boost the engine with a favorable pressure gradient (p02>p03) and without mechanical losses increment due to the excessive usage of the scavenge pump. During the modelling stage, several iterative loops for a complete parametric study were done. The variables selected to find an optimum solution were several, including: VT&VCM configurations, p02/p03, engine rpms and λ.

Figure 15 shows the best-found solution: an intermediate VT&VCM position (CR=8.2) and λ=1.64. First, the targeted power of 30 kW or more is achieved in a wide operative engine region (dashed circle in Figure 15_A). Secondly, the intermediate engine CR helps in a high degree in lowering the maximum cylinder temperature, for NOx generation avoidance (dashed circle in Figure 15_B). Thirdly, the early exhaust ports opening corresponding to the engine CR of 8.2 (see in Figure 1_B exhaust advance dependency with mechanism position) raises exhaust temperature up to the 725 ºC required to help the boosting duty. Finally, shaded area is the one that accomplishes all the requirements and provides with an ISFC of 206-208 g/kWh. Approximately an improvement of 10 g/kWh (a 4.6 % improvement) with respect to the ISFC of the direct injection configuration with stoichiometric mixture. The operative area that fits all the requirements is with an engine speed range about 3300 to 4000 rpm, as previously stated, the 2S-ROPE mechanical losses should be reduced thanks to the downspeeding approach (see Figure 2).

To evaluate the viability of boosting the engine in such a way that p02/p03 is kept around 1.30 to 1.40. The same methodology as the one in the previous section is followed. The values of p02 are imposed to be 1.30 and 1.40 times p03 at equation (11) and it was evaluated for the system. T03 is taken from the simulations on Figure 15_C (725ºC in the shaded area). And finally, p4 and p01 are taken from iso-mass-flow working points from the reference 4S-TSI-DI engine.

The resulting continuous trends in Figure 16 show for both p02/p03 the required turbocharger efficiency. Dashed lines show the p02/p01 required to reach the p02 demand for each turbine pressure ratio (p03/p4). Taking again as a reference point A from Figure 14 one can realize how far the desired p02/p03 is highly unrealistic: in other words, T03 it is too low, or the required turbocharger efficiency is higher than available technology to target the desired p02/p03. This implies the intensive use of an auxiliar mechanically or electrically driven compressor (higher mechanical losses).

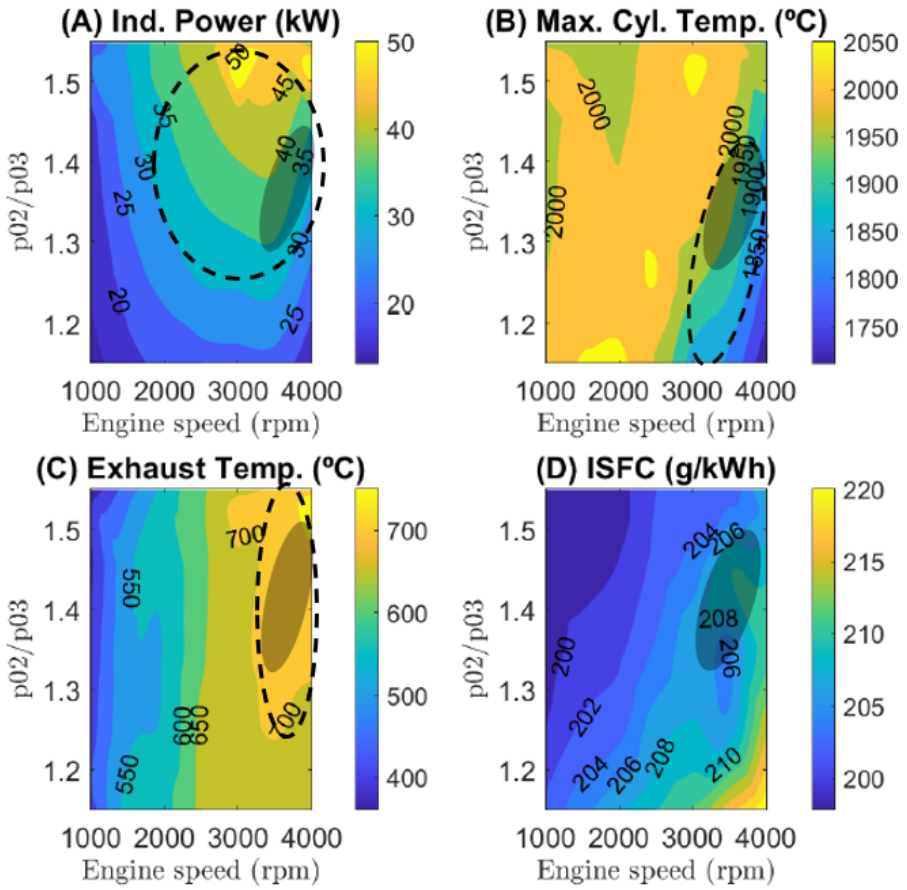

Figure 15: Lean combustion and direct injection simulation results for fixed VCR of 8.2. Different variables evolution as a function of the p02/p03 and engine speed. (A) Shows indicated power. (B) Shows maximum cylinder temperature. (C) Shows exhaust temperature. (D) Shows indicated brake specific consumption

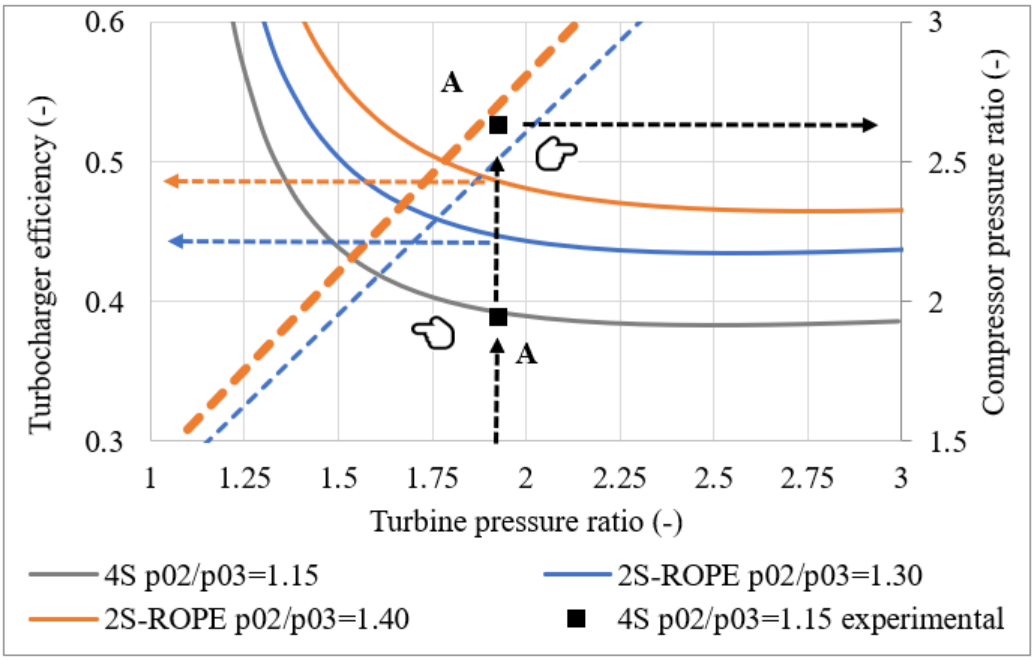

Figure 16: Turbocharger efficiency and resulting boost pressure for different exhaust pressure values. 2S-rope T03/T01=998.15/293.15

5. Conclusions

A new 2S-ROPE concept has been manufactured, assembled, and tested. This engine has been designed from the drawing table to operate as a range extender for automotive application under series hybrid configurations (e-REX series of 2S-ROPE). The experimental campaign has been taken as a reference to partially validate the main engine kinematics, ports timing, piping modelling and combustion with the purpose of calibrating an in house developed 1D gas-dynamics model for further potential and performance research.

The 2S-ROPE engine tested was SI, port fuel injection, and with scavenge pump assistance. No misfiring was measured, but combustion variability was slightly higher in comparison to a SI 4-stroke engine already available in the market. Lack of combustion efficiency was attributed to the short-circuit, what was later confirmed in the modelling campaign.

Although the available experimental information was limited, it was enough for validating a 1-D gas-dynamic model, with further objective of performing a prospective study of different turbocharging and injection technologies. Direct fuel injection, lean combustion and turbocharging were explored through 1-D gas-dynamic simulation to calculate the potential advantage when avoiding fuel short-circuit. The three main conclusions achieved are:

1. With port fuel injection configuration, it is necessary to guarantee close to perfect displacement during the scavenging process. Otherwise emissions and fuel consumption figures are unacceptable. Even if perfect displacement is ensured, the

operative area that guarantees 100 % trapping efficiency is much reduced in terms of scavenging pressure and rpm. On the contrary, the final solution would result in a very simple and affordable range extender engine for series hybrid vehicles. The resulting range extender is proposed to be connected to the electric generator, without gear box, at 3500 rpm, where a maximum power value of 32 kW is obtained. The VT&VCM system allows a load control that ranges between 32 kW and 24 kW: a 25% load control capability without throttling and keeping a constant ISFC around 250 g/kWh.

2. If direct fuel injection is selected, the operative area in terms of power and fuel consumption is widened. However, the usage area of a 3W catalyst is again reduced to the area with 100% trapping efficiency. Boosting the engine to the required p02/p03 by means of a turbocharger it is possible with nowadays turbocharger technology, limiting the use of scavenge pump to engine starting and few other off-design operations. The ISFC in these working areas corresponds to approximately 216 - 220 g/kWh, the indicated power is slightly increased to 35 kW and again engine speed in the range of 3500 rpm allows avoiding the use of gear box to connect to the electric generator.
3. If NOx generation is to be avoided, lean combustion it is necessary. After an iterative procedure of optimization, it was found that a λ=1.64 may avoid NOx production. The operative area achieves the target indicated power of 35 kW with an ISFC of 205 g/kWh, what represents a 4.6 % improvement with respect stoichiometric conditions. It was also explored the viability of obtaining the required p02/p03 ratio exclusively by a turbocharger. It was concluded that turbocharger required efficiency would be too high in comparison to nowadays technology. An auxiliary system helping with the boosting duty would be required, however this would imply some extra mechanical losses that may dilute the 4.61% of ISFC improvement over the stoichiometric mixture option.

6. Acknowledgments

Alejandro Gómez Vilanova is partially supported through contract: Ayuda de Formación de Profesorado Universitario (FPU18/04811).

The authors wish to thank Roberto Lendaro his continuous and enthusiastic economical support to INNengine project and to Raul Luján for his invaluable work during the experimental campaign. It was also of great help the contribution of José Luis Galiana Amorós during the setup and the calibration of the modelling tools.

The authors also wish to thank Agencia IDEA (Agencia de Innovación y Desarrollo de Andalucía) which depends on Consejería de Economía, Conocimiento, Empresas y Universidad through PROGRAMA DE APOYO A LA I+D +i EMPRESARIAL (code 402C1700011) and subsidy in a non-competitive competition regime for companies for industrial development, improvement of competitiveness, digital transformation and job creation in Andalucía (401N1800210)

7. References

[1] Mujkic E, Klingner D. Dieselgate: How Hubris and Bad Leadership Caused the Biggest Scandal in Automotive History. Public Integr 2019;21:365–77. https://doi.org/10.1080/10999922.2018.1522180.

[2] Qian Y, Li Z, Yu L, Wang X, Lu X. Review of the state-of-the-art of particulate matter emissions from modern gasoline fueled engines. Appl Energy 2019;238:1269–98. https://doi.org/10.1016/j.apenergy.2019.01.179.

[3] Luján JM, Serrano JR, Piqueras P, Diesel B. Turbine and exhaust ports thermal insulation impact on the engine efficiency and aftertreatment inlet temperature. Appl Energy 2019;240:409–23. https://doi.org/10.1016/j.apenergy.2019.02.043.

[4] Bozza F, De Bellis V, Teodosio L. Potentials of cooled EGR and water injection for knock resistance and fuel consumption improvements of gasoline engines. Appl Energy 2016;169:112–25. https://doi.org/10.1016/j.apenergy.2016.01.129.

[5] Kirwan JE, Shost M, Roth G, Zizelman J. 3-Cylinder Turbocharged Gasoline Direct Injection : A High Value Solution for Low CO2 and NOx Emissions. vol. 3, SAE International; 2018. https://doi.org/https://doi.org/10.4271/2010-01-0590.

[6] Galindo J, Luján JM, Serrano JR, Dolz V, Guilain S. Design of an exhaust manifold to improve transient performance of a high-speed turbocharged diesel engine. Exp Therm Fluid Sci 2004;28:863–75. https://doi.org/10.1016/j.expthermflusci.2004.01.003.

[7] Smith JK, Roberts P, Kountouriotis A, Richardson D, Aleiferis P, Ruprecht D. Thermodynamic modelling of a stratified charge spark ignition engine. Int J Engine Res 2020;21:801–10. https://doi.org/10.1177/1468087418784845.

[8] Benajes J, Novella R, Gomez-Soriano J, Martinez-Hernandiz PJ, Libert C, Dabiri M. Evaluation of the passive pre-chamber ignition concept for future high compression ratio turbocharged spark-ignition engines. Appl Energy 2019;248:576–88. https://doi.org/10.1016/j.apenergy.2019.04.131.

[9] Redon F, Kalebjian C, Kessler J, Rakovec N, Headley J, Regner G, et al. Meeting stringent 2025 emissions and fuel efficiency regulations with an opposed-piston, light-duty diesel engine. SAE Tech. Pap., vol. 1, 2014. https://doi.org/10.4271/2014-01-1187.

[10] Wang X, Zhao H. Effect of piston shape design on the scavenging performance and mixture preparation in a two-stroke boosted uniflow scavenged direct injection gasoline engine. Int J Engine Res 2020. https://doi.org/10.1177/1468087419900072.

[11] Ma F, Zhao C, Zhang S, Wang H. Scheme Design and Performance Simulation of Opposed-Piston Two-Stroke Gasoline Direct Injection Engine. SAE Tech. Pap., vol. 2015- April, 2015. https://doi.org/10.4271/2015-01-1276.

[12] Abdul-Manan AFN, Won HW, Li Y, Sarathy SM, Xie X, Amer AA. Bridging the gap in a resource and climate-constrained world with advanced gasoline compression-ignition hybrids. Appl Energy 2020;267:114936. https://doi.org/10.1016/j.apenergy.2020.114936.

[13] Geng W, Lou D, Wang C, Zhang T. A cascaded energy management optimization method of multimode power-split hybrid electric vehicles. Energy 2020;199:117224. https://doi.org/10.1016/j.energy.2020.117224.

[14] García A, Monsalve-Serrano J, Martínez-Boggio S, Wittek K. Potential of hybrid powertrains in a variable compression ratio downsized turbocharged VVA Spark Ignition engine. Energy 2020;195:117039. https://doi.org/10.1016/j.energy.2020.117039.

[15] Mehta S, Hemamalini S. A Dual Control Regenerative Braking Strategy for Two-Wheeler Application. Energy Procedia 2017;117:299–305. https://doi.org/10.1016/j.egypro.2017.05.135.

[16] Garrido Requena J. EP 3 066 312 B1. Spain, Barcelona: European Patent Office; 2013.

[17] Garrido Requena J. e-REX. The True Range Extender by INNengine (English version) 2020. https://www.youtube.com/watch?v=6wT87IqheV0 (accessed June 18, 2020).

[18] Herold RE, Wahl MH, Regner G, Lemke JU, Foster DE. Thermodynamic benefits of opposed-piston two-stroke engines. SAE Tech. Pap., 2011. https://doi.org/10.4271/2011-01-2216.

[19] Bermúdez V, Tormos B. Pérdidas mecánicas. In: Payri González F, Desantes Fernández JM, editors. Mot. Combust. interna Altern., Valencia: Editorial UPV; 2011, p. 152–72.

[20] Egnell R. Combustion diagnostics by means of multizone heat release analysis and NO calculation. SAE Tech Pap 1998. https://doi.org/10.4271/981424.

[21] Pla B, De la Morena J, Bares P, Jiménez I. Cycle-to-cycle combustion variability modelling in spark ignited engines for control purposes. Int J Engine Res 2019. https://doi.org/10.1177/1468087419885754.

[22] Payri F, Molina S, Martín J, Armas O. Influence of measurement errors and estimated parameters on combustion diagnosis. Appl Therm Eng 2006;26:226–36. https://doi.org/10.1016/j.applthermaleng.2005.05.006.

[23] Armas O, Rodríguez J, Payri F, Martín J, Agudelo JR. Effect of the trapped mass and its composition on the heat transfer in the compression cycle of a reciprocating engine. Appl Therm Eng 2005;25:2842–53. https://doi.org/10.1016/j.applthermaleng.2005.02.007.

[24] Martin J, Arnau F, Piqueras P, Auñon A. Development of an Integrated Virtual

Engine Model to Simulate New Standard Testing Cycles. SAE Tech Pap 2018;2018-April:1–17. https://doi.org/10.4271/2018-01-1413.

[25] Sturm S, Schmidt S, Kirchberger R. Overview of Different Gas Exchange Concepts for Two-Stroke Engines. SAE Tech. Pap., 2018, p. 1–11. https://doi.org/10.4271/2018-32-0041.

[26] Serrano JR, Olmeda P, Arnau FJ, Samala V. A holistic methodology to correct heat transfer and bearing friction losses from hot turbocharger maps in order to obtain adiabatic efficiency of the turbomachinery. Int J Engine Res 2019. https://doi.org/10.1177/1468087419834194.

[27] Wagner U, Eckert P, Spicher U. Possibilities of simultaneous in-cylinder reduction of soot and NOx emissions for diesel engines with direct injection. Int J Rotating Mach 2008;2008. https://doi.org/10.1155/2008/175956.

[28] Xu G, Wright YM, Schiliro M, Boulouchos K. Characterization of combustion in a gas engine ignited using a small un-scavenged pre-chamber. Int J Engine Res 2018. https://doi.org/10.1177/1468087418798918.

[29] Toulson E, Schock HJ, Attard WP. A review of pre-chamber initiated jet ignition combustion systems. SAE Tech. Pap., 2010. https://doi.org/10.4271/2010-01-2263.